Topology optimization applied an threshing separation rotor component

Aquiles S. Schauenberg [1], Ederval S. Lisboa[1], Maikson L. P. Tonatto [1]

[1] *Group on Mechanics of Materials and Structures (GMEC), Federal University of Santa Maria*
Rod. Taufik Germano, nº 3013, 96503-205, Rio Grande do Sul, Brasil
maikson.tonatto@ufsm.br

Abstract. Threshing separation rotors are extensive used as extensively in a combine harvester as a flow separator that includes at least one rotary axis. Among the components of the rotor, the finger is one of the main ones because it is responsible for separating the grains and the straw. Nonetheless, the optimization is little explored which makes it a component of low structural performance. This work aims to develop a topology optimization using a finite element (FE) model in order to reduce the mass of the finger. In the first step, the model is performed considering the pre-torque of the screw and the bending load that the straw generates on the finger. Besides, the normal and tangential contacts are considered between the components. Then, the topology optimization is performed by Solid Isotropic Material with Penalization (SIMP) method. The objective function is defined as minimizing the volume of the finger subject to von Misses stress and displacement constraints. The topology optimization results present that the volume reduced achieve 84% in comparation with original model.

Keywords: SIMP optimization; Finite Element model; Threshing separation rotor.

1 Introduction

It's recognizable the necessity of investments in new technologies in the field of grain production due the increase of demand. In combine harvesters, the rotor is a flow separator fixed longitudinally on axis of combine and enclosed by concave grids as shown on Fig. 1. The spiral component (item 1) rotates around the axis and moves the grains longitudinally. This movement is induced due to the interaction between the rotor (item 2) and external concave grids, according Brian [1] and Srivastava [2]. Topology optimization method has been used as an important tool to develop mechanical components with efficiency in automotive and aircraft industries. For example, Cavazzuti [3] and Zhuang [4] performed the topology optimization on car frame and a gearbox, respectively. Zhu [5] applied the topology optimization on aircraft design and airspace structures. Chu [6] develop a new approach to reduce volume in structures. However, in the agricultural industry, there are still several components little explored which make them an inefficient product, such as the rotor separator.

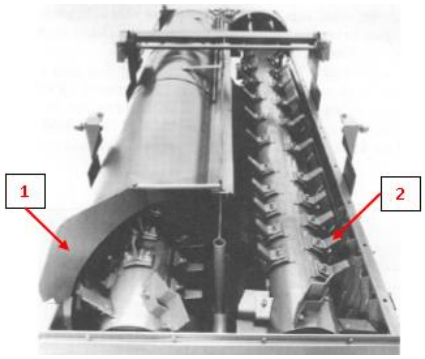

Figure 1. Threshing separation rotor [3].

This study aims to perform a topology optimization of threshing separation rotor of a combine, specifically the rotor finger component. A finite element (FE) model is performed in order to obtain the mechanical behavior of original rotor subject to flexural load and then used in optimization process. The objective function is minimizing the volume of finger and the stress and displacement are used as constraints.

2 Finite element (FE) model

The rotor finger is composed by two parts (finger and protective case), in which the properties of each component are described in Tab. 1. The materials applied on the finger and protective case are low alloy carbon steel (SAE 1010) and Chromium and Manganese alloy (SAE 4130) , respectively. To aid the model validation and avoid excessive computational time, it is considered that the fastening assembly (nut, washer and screw) that makes the connection between the two parts is a single component, this process is done by joining the parts.

Table 1. Properties of materials.

Property	SAE 1010 [7]	SAE 4130 [8]	Unit
Yield stress	245	436	MPa
Tensile strength	350	669	MPa
Density	7900	7850	kg/m^3
Elastic modulus	179000	205000	MPa
Poisson's ratio	0.29	0.25	-

Figure 2 shows the FE model of threshing separation rotor. The surface-surface interaction between finger and protective case are used, due the intermediate area is the place where the greatest interaction between the components occurs, as shows in Fig. 2a. This contact properties have frictionless tangential and hard normal behavior. The bonded contacts are used between bolt and protective case and nut and finger, where movement restrictions are imposed on each surface, as shown in Fig. 2b.

Regarding the boundary conditions, the bottom area of the finger is welded to the tube, so an encastred is applied in this region, as shows in Fig. 2c. Two steps are created where applied the loads. For both steps, a maximum value of 100 iterations is applied, with increments at each iteration of 10%. Both steps were generated as a static procedure and with Newton Raphson's solution technique. In the step one, a pre-load in bolt is applied in order to create the contact compressive force between protective case and finger, as shows in Fig. 2c. In the step two, this pre-load is propagate and a flexural load is create. The flexural load is applied on area of 35.5×50 mm². In order to apply this load in area, a coupling constraint is created with rigid beam elements that connect a reference point (RP) and the nodes of the area, as shows in Fig. 2b. The flexural force is then applied in the positive direction of the Z axis, as shows Fig. 2d.

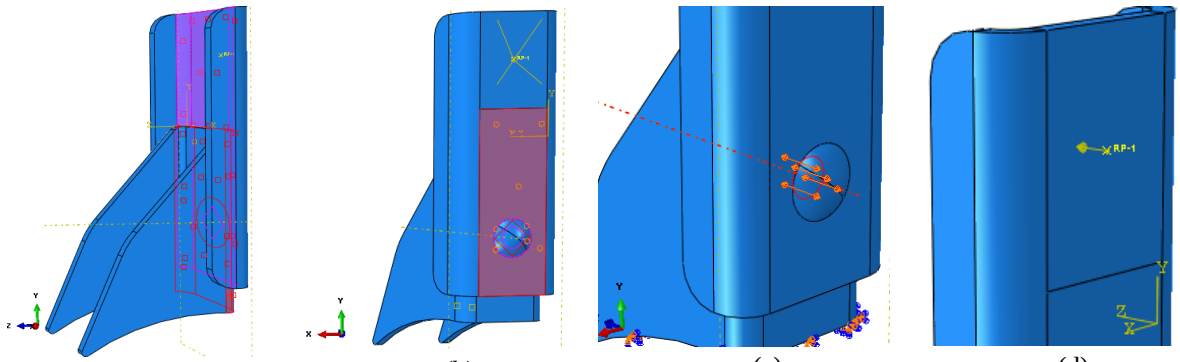

(a) (b) (c) (d)

Figure 2. FE model: (a) protective case-finger contact, (b) bolt-protective case contact. (c) axial pre-load applied in the bolt. (d) flexural force applied to RP.

The convergence mesh is performed with elements between 0.5 mm and 4 mm. Afterwards, the mesh convergence of each element is analyzed to define the element that best relates computational processing time and value accuracy. A mesh refinement is also carried out in the area where the topology optimization will be applied. The finger uses a mixture of elements of the type C3D10 (tetrahedron) and C3D8R (hexahedron), as shown in Fig. 3a. Hexahedral elements are used in the finger protective case (Fig. 3b) and tetrahedral elements are used in the bolt and nut (Fig. 3c). At least 4 elements will be used along of thickness of the protective case and finger.

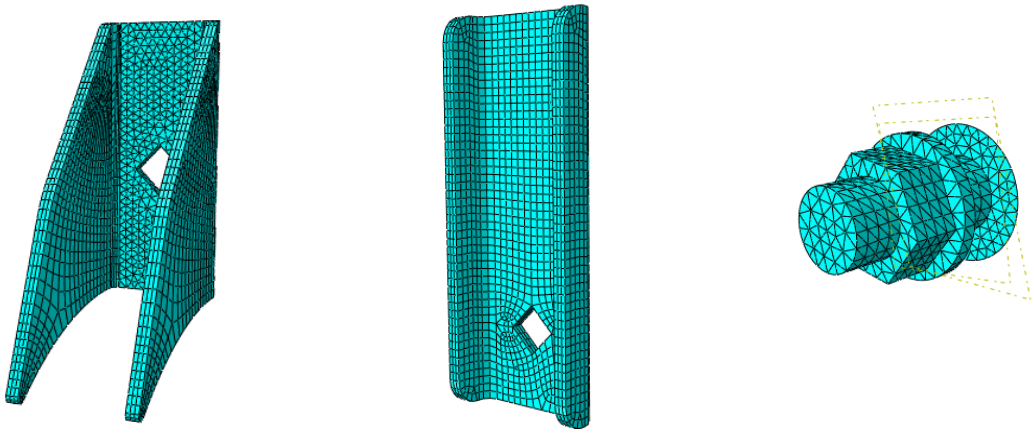

(a) (b) (c)

Figure 3. (a) Mesh on the finger, (b) mesh on the protective case and (c) mesh on the nut and bolt assembly.

3 Topology optimization

For the topology optimization process to be defined it is necessary to implement the results found in the FE model, specifically vom Misses stresses and displacements. The optimization problem consists of an objective function that minimize the volume and subject to stress and displacement constraints according to Eq. 1:

$$\text{min} \quad V = \sum_{e=1}^{N} V_e \, \rho_e$$

$$\text{subject to} \quad (\sigma_e)_{VM} \leq \rho_e^p \sigma_l \text{ if } \rho_e > 0 \text{ and } E = \rho_e{}^p \cdot E^0 \,, \qquad (1)$$

$$u_z \leq \rho_e^p u_{max}^z \text{ if } \rho_e > 0,$$

$$0 < \rho_{min} \leq \rho_e \leq 1, \quad e = 1, \ldots, N.$$

where V is the total volume, V_e is the volume of each element, ρ_e is the artificial density in each element, $(\sigma_e)_{VM}$ is the von Mises stress of the model, p is the penalty factor of the SIMP method, σ_l is the yield stress of the material, E^0 and E are the constitutive tensors of the initial and final volume respectively, u_z is the displacement in the Z direction of the analyzed node, u_{max}^z is the maximum displacement allowed and ρ_{min} is the minimum artificial density, as mentioned by Bendsoe [9].

The objective function is minimize the volume (V) in the lateral regions of the finger (area of interest). This area is chosen due it does not have any contact conditions, also due it is a surface with greater volume in the model. The SIMP method is used with a penalty factor (p) equal to 3. This objective function is subject to stress and displacement constraints. The first constraint defined is the yield stress in the optimization area (σ_e). According to Norton's definition [10], the safety factor for ductile materials over stress limit must be greater or equal to 3, so the limit stress for optimization (σ_l) is an allowable stress equal to yield stress divided by safety factor. The second constraint is applied to the displacement at RP, that is, the displacement generated by the bending force in the direction of the Z axis (u_z). Permissible percentages of the original displacement are created as shown in Tab. 2, so it is possible to analyze how the removal of material is made in the different displacement constraints.

The RP was chosen due it is a point with high displacement compared to other nodes. Therefore, in order to

remove material in the area of interest, the displacement at point RP on the z axis cannot be greater than or equal to a given maximum displacement value (u^z_{max}). The maximum displacement (u^z_{max}) allowed is defined as the displacement observed in the original model.

Table 2. Different displacement and stress constraints.

Model	Nomenclature	Displacement (u^z_{max})	Stress (σ_l)
1	ot_1	$u_z \leq u^z_{max} * 0{,}15$	$(\sigma_e)_{VM} \leq \frac{\sigma_e}{3}$
2	ot_2	$u_z \leq u^z_{max} * 0{,}5$	
3	ot_3	$u_z \leq u^z_{max} * 2$	

4 Results and discussions

The flexural load (F_{max}) applied on the finger is obtained through the contact between the chaff of the grain the fingers. The torque of harvester motor is transmitted through of several pulleys and one transmission box with double reduction, resulting in a torque T of 606 N.m in tube that the fingers are connected. Therefore, as the radius from the center of the tube to the end of the finger protective case (r) is 0.272 m, the maximum load acting on the rotor fingers can be found as $F_{max} = T/r = 2227.94$ N, according to Halliday [11]. The rotor has 38 fingers, so the flexural load on each finger (F_f) is the maximum force across the entire threshing separation rotor distributed between the number of fingers in the tube, considering ideal working conditions, the input and output flow in the rotor is constant, making all fingers work with the same applied load. A safety factor of three is considered for agricultural implements. Therefore, the flexural load on each finger is given by, $F_f = (F_{max}/38) \times FS \approx 180$ N.

The pre-load (F_i) in bolt is calculated by $F_i = 0{,}75 \cdot F_p$, where F_p is the proof load. The proof load of bolt is calculated by $F_p = 0.9 \cdot S_y \cdot A_s$, where S_y is the yield stress of bolt equal to 640 MPa and A_s is the area under tension equal to 84.3 mm², therefore $F_p = 48557\ N$ and $F_i = 36418$ N. This procedure is obtained according Shigley [12].

Mesh convergence is done using five different sizes of elements, being observed the flexural load vs. displacement curves. In this case, a flexural load equal to 3500 N is in order to obtain large displacement. The displacement is obtained at RP. The coarse mesh of 4 mm elements is refined gradually until fine mesh of 0.5 mm element. The flexural load vs. displacement curves are shows in Fig. 4, where the minimum difference is observed, mainly between meshes 1, 2, 4 and 5, indicating the convergence of these meshes.

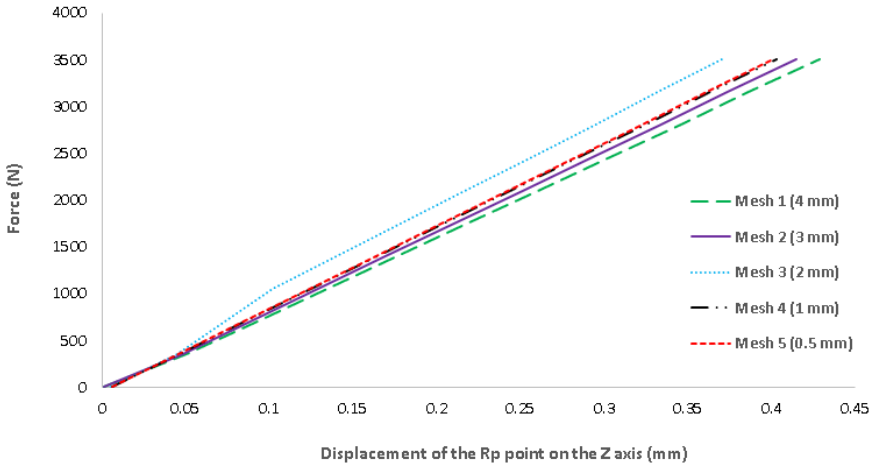

Figure 4. Force vs. displacement curve for different refinement of mesh.

To choose the element, computational time is analyzed, where in the meshes 4 and 5 is noticed higher computation cost between analyzed, Therefore, the mesh 2 is used in the models due their good balance between computation cost and accuracy.

The stress field in the original finger is shows in Fig. 5. Fig. 5a shows the stress filed in the end of step 1 where is applied the pre-load in the bolt. It is observed that the von Mises stress is maximum closed the bolt region, where the legend is limited in 640 MPa (yield stress of bolt) to better visualize the results. It is observed that some regions presents stress concentrations due the discontinuities of the elements, producing infinity stress in a small area. Fig. 5b shows the stress field in end of step 2 (pre-load+flexural load), where the legend is limited in 140 MPa (stress used as constraint in the topology optimization). It was noted that the flexural load does not generate high stress, where the maximum stress at finger (≈23 MPa) is located closed at the top region in the radii of curvature.

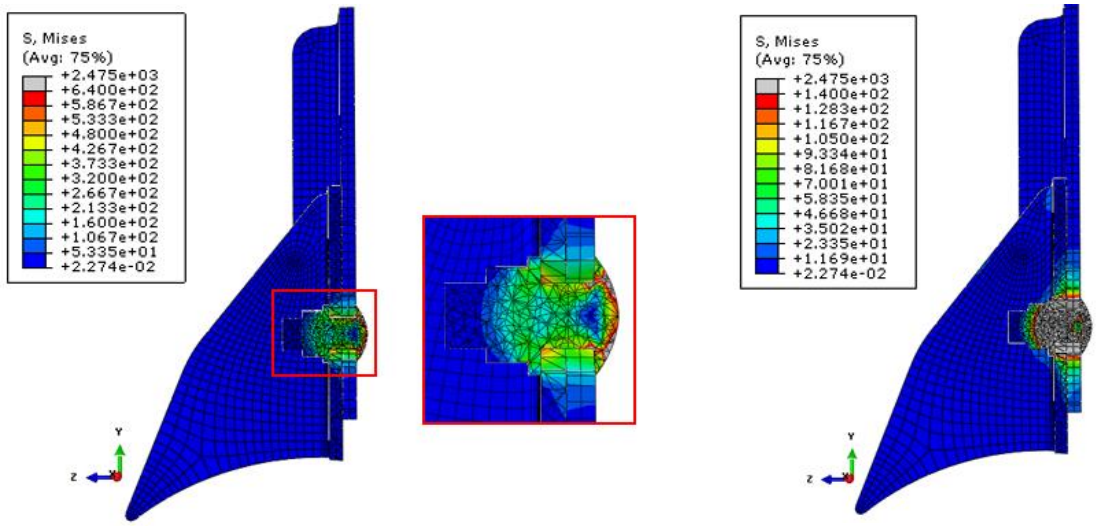

(a) (b)

Figure 5. (a) Stress field in the end of step 1 (pre-load) and (b) stress field in the end of step 2 (pre-load+flexural load).

The flexural load vs. displacement curve found during the step 2 of the original model is shows in Fig. 6. It is noted a non-linearity of curved, mainly around 40 N. This behavior is attributed to the effects caused by pre-load in the bolt. The pre-load in step 1 causes a small gap between the protective case and the finger.

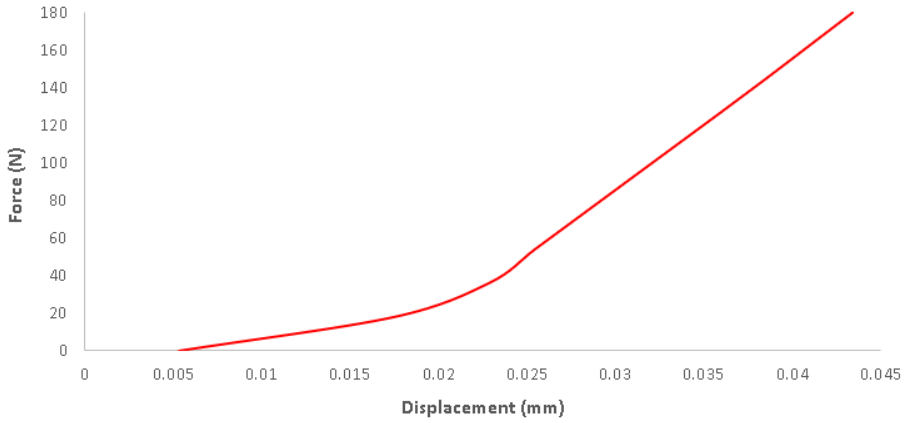

Figure 6. Flexural load vs. displacement at RP curve during step 2.

When the flexural load is applied in step 2, this gap facilities the deformation of finger, creating a zone of lower stiffness in the beginning of the curve until of displacement of ≈0.02 mm. In this displacement level, the contact between protective case and finger is stablish again and a region of the curve with high stiffness occurs for displacements above ≈0.02 mm. It is noted that the maximum displacement observed at point RP is 0.0434 mm corresponding the maximum flexural load applied. This maximum displacement is used as constraint in topology

optimization.

Regarding the topology optimization, all models need of thirty interactions in order to obtain the objective function converge. Fig. 7a shows the convergence curves obtained in each model. It is observed that until the twentieth interaction there is a greater reduction in volume and from this interaction the objective function stabilizes. Fig. 7a shows the evolution of displacement and stress constraints in function of interactions. The stress constraint in models ot_1 and ot_2 assuming almost constant values until the model reaches convergence. In other hand, the model ot_ 3 demonstrated greater variation. The displacement constraint of the three models present variation until fifth interaction and from this interaction, the displacement assumes almost constant values.

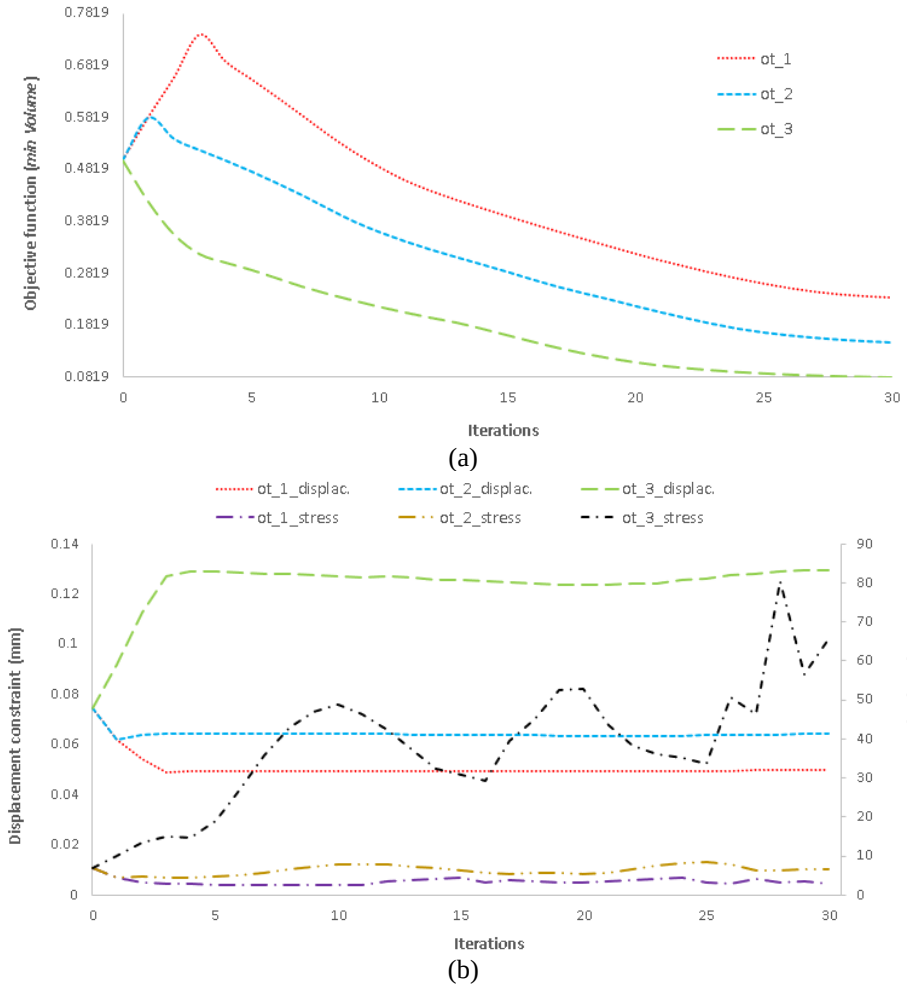

Figure 7. (a) Objective function convergence curves and (b) evolution of the displacement and stress constraints for different models.

Figure 8 shows the final shape of topology optimization in the three evaluated models. Similar shape is found for all models, where it is noticed that the material is removed in larger proportion closed of inner area of the finger. This is attributed that this region is subject to low stress. It is also noted that in these optimized models present similar shape of the truss, where the external contour is connected with internal reinforcements. It is noted that the material removed increased when the maximum displacement is increased (from model ot_1 to ot_3). In the model ot _3, a larger reduction in the thickness of the optimized area is visualize, where the reinforcement element is almost completely removed. In all models, the complex geometries are created where a shape optimization might be needed to facilitate manufacturing. Besides, it is noted that material removed in the models is proportional to the displacement constraint imposed. Less material mass is needed to make the structure stiffness, when the displacement at point RP increase. The stress constraint does not have a great influence on the shape geometry, as it is constant in all models. The volume removed from the area of interest and the final mass of each model are described in Tab. 3.

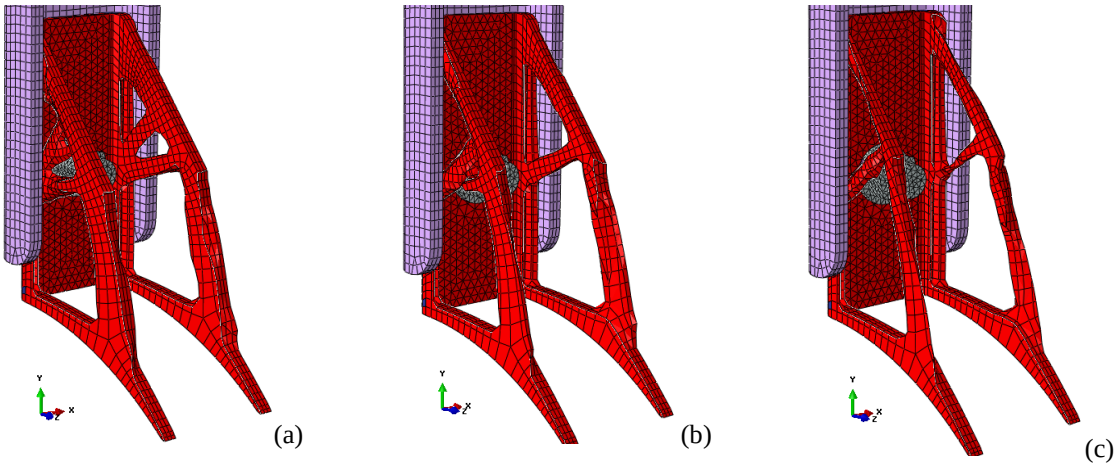

Figure 8. Final shape of the topology optimization: (a) model ot_1, (b) model ot_2 and (c) model ot_3.

Table 3. Mass and volume of original and optimized models.

Nomenclature	Total mass (kg)	Volume reduced (%)
Original model	0.402	–
ot_1	0.262	53
ot_2	0.217	70
ot_3	0.182	84

5 Conclusions

This study performed a topology optimization in order to minimize volume of three different models of a threshing separation rotor used as component of a combine harvesters. A finite element model is used in order to obtain the stress and displacement used in topology optimization process. In general, the topology optimization with displacement and stress constraints applied to the finger of the rotor presents efficient to material reduction, which can bring better performance for the component as well as a possible reduction in material and construction costs. Between the models optimized, it is observed that the maximum volume reduced is 84% in comparation with original model. Besides, it was noticed that in all models highly complex geometries are created where due this characteristic, a shape optimization or a remodeling in order to remove corners and thin regions should be necessary to facilitate the production of the parts.

References

[1] H. Brian, “Crop engaging elements for a combine harvester separating rotor”. Patent, 2012.
[2] A. Srivastava *et al. Engineering Principles of Agricultural Machines*. 2 ed. American Society of Agricultural and Biological Engineers, 2012.
[3] M. Cavazzuti *et al.* “High performance automotive chassis design: A topology optimization based approach”. *Structural and Multidisciplinary Optimization*, vol. 44, n. 1, pp. 45–56, 2011.
[4] S. Zhuang. “Gearbox housing topology optimization with respect to gear misalignment”. *International Journal of Mechanical Engineering and Robotics Researchr*, 2012.
[5] J. Zhu, S. Zhuang and L. Xia. “Topology Optimization in Aircraft and Aerospace Structures Design”. *Archives of Computational Methods in Engineering*, 2016.
[6] S. Chu, L. Gao *et al.* “A new method based on adaptive volume constraint and stress penalty for stress-constrained topology optimization”. *Structural and Multidisciplinary Optimization*, 2018.
[7] O. Bilir. “The relationship between the parameters C and n of Paris' law for fatigue crack growth in a SAE 1010 steel”. *Engineering Fracture Mechanics*, 1990.
[8] O. Heidary, O. Mirzaee, *et al.* “UP-quenched SAE 4130 steel: Mechanical properties assessment and bainite formation”. *Materials Science and Engineering*, 2020.
[9] M. P. Bendsoe *et al. Topology Optimization Theory, Methods and Applications.* 1 ed. Nova York, 2003.
[10] L. R. Norton. *Projeto de máquinas: Uma abordagem integrada*. 4 ed. BOOKMAN EDITORA LTDA, 2013.
[11] R. Resnick and D. Hallyday. *Física.* 4 ed. Livros técnicos e científicos editora LTDA, 1983.
[12] J. E. Shigley *et al. Projeto de engenharia mecânica.* 7 ed. São Paulo, 2005.